Materials Research. 2019; 22(2): e20180639
DOI: http://dx.doi.org/10.1590/1980-5373-MR-2018-0639

Production and Characterization of a Silica-Alumina Membrane Using Novel Tubular Freeze-Cast Substrates

***Daniel Dornellas Athayde*[a]*, *Ana Clara Amado Dolabella*[b], *Bruno Cunha Dias*[a],**

***Bruno Maciel Sousa*[a], *Débora Guimarães da Silva*[a], *Daniela Cordeiro Leite Vasconcelos*[a],**

***Wander Luiz Vasconcelos*[a]**

[a]*Departamento de Engenharia Metalúrgica e de Materiais, Universidade Federal de Minas Gerais - UFMG, Avenida Presidente Antônio Carlos, 6627, 31270-901, Belo Horizonte, MG, Brasil*
[b]*Departamento de Engenharia Química, Universidade Federal de Minas Gerais - UFMG, Avenida Presidente Antônio Carlos, 6627, 31270-901, Belo Horizonte, MG, Brasil*

Received: September 25, 2018; Revised: December 20, 2018; Accepted: January 07, 2019

Development of new ceramic membranes has recently grown due to its superior thermal and mechanical stability. An interesting approach to manufacture asymmetric membranes is the production of aligned pore structure by the freeze-casting method. The lack of studies involving membrane production with tubular freeze-cast substrates warrants more research. In this study, a novel tubular freeze-cast alumina substrate was used for deposition of a silica top layer. The substrate showed radially aligned pores, indicating precise structure control. The obtained pore structure shows high potential for membrane manufacture. The silica layer was produced by the sol-gel method and dip-coated on the substrates with two different withdrawal speeds. The microporous silica showed pores smaller than 2 nm. The highest withdrawal speed resulted in broader substrate coverage. However, a uniform silica layer was only obtained after a second deposition. These results confirm the viability to use tubular freeze-cast substrates for production of nanofiltration membranes.

Keywords: *Freeze-casting, Tubular Substrates, Sol-gel, Asymmetric Membranes.*

1. Introduction

Porous ceramic membranes have been widely studied in the last decades for a variety of separation processes, such as gas separation [1-3]. The improved thermal and chemical stability of inorganic materials, when compared to polymeric, suggests potential for applications under industrial conditions [4]. These membranes consist of a physical porous barrier that allows permeation of a fluid while hindering the passage of larger molecules. For instance, the molecular sieve mechanism allows passage of small gas molecules (H_2), while retaining the large molecules (N_2) [2]. Thus, an important aspect of these porous materials is the pore size of the membranes. Table 1 details the typical particle size exclusion and pressures for the different membrane categories, ranging from sizes smaller than 1 nm for reverse osmosis to 10,000 nm for microfiltration [5-8]. The pore sizes dictate the ability of the membrane to separate the substances and, thus, have a great impact on the membrane selectivity.

Among the membrane geometries available, the asymmetric membrane has shown impressive results [9]. This geometry consists on a macroporous substrate with a thin top layer. The support provides mechanical strength to the membrane and must show low resistance for mass transport through its pores. The top layer is responsible for the separation and selectivity of the membrane and should be as thin as possible [1,10]. However, methods conventionally used to prepare the ceramic substrate produce a tortuous pore structure with isolated and dead-end pores [11]. These are detrimental to the mass transport and, thus, undesirable. The freeze-casting technique is an interesting alternative to overcome these issues [12]. It allows production of substrates with aligned pore structure and precise control of the pore shape when different solvents are used [13].

Table 1. Typical values of pore size and pressures used on membrane separation methods.

Separation method	Particle size exclusion (nm)[5,6]	Pressures (bar)[7,8]
Microfiltration	100 – 10,000	0.7 – 3
Ultrafiltration	2 – 100	1 – 10
Nanofiltration	0.1 – 2	7 –30
Reverse osmosis	<1	20 – 100

As shown in Figure 1, the freeze-casting consists on controlled freezing of a ceramic slurry with aqueous or organic solvent. The slurry is submitted to a cold media (i.e. liquid nitrogen) leading to a temperature gradient. The solvent crystals then begin to grow in the temperature gradient direction, establishing an organized structure. When the solvent is completely frozen, the structure shows aligned solvent crystals with ceramic particles entrapped between them. The chosen solvent has a great impact on the shape

*e-mail: ddathayde@gmail.com.

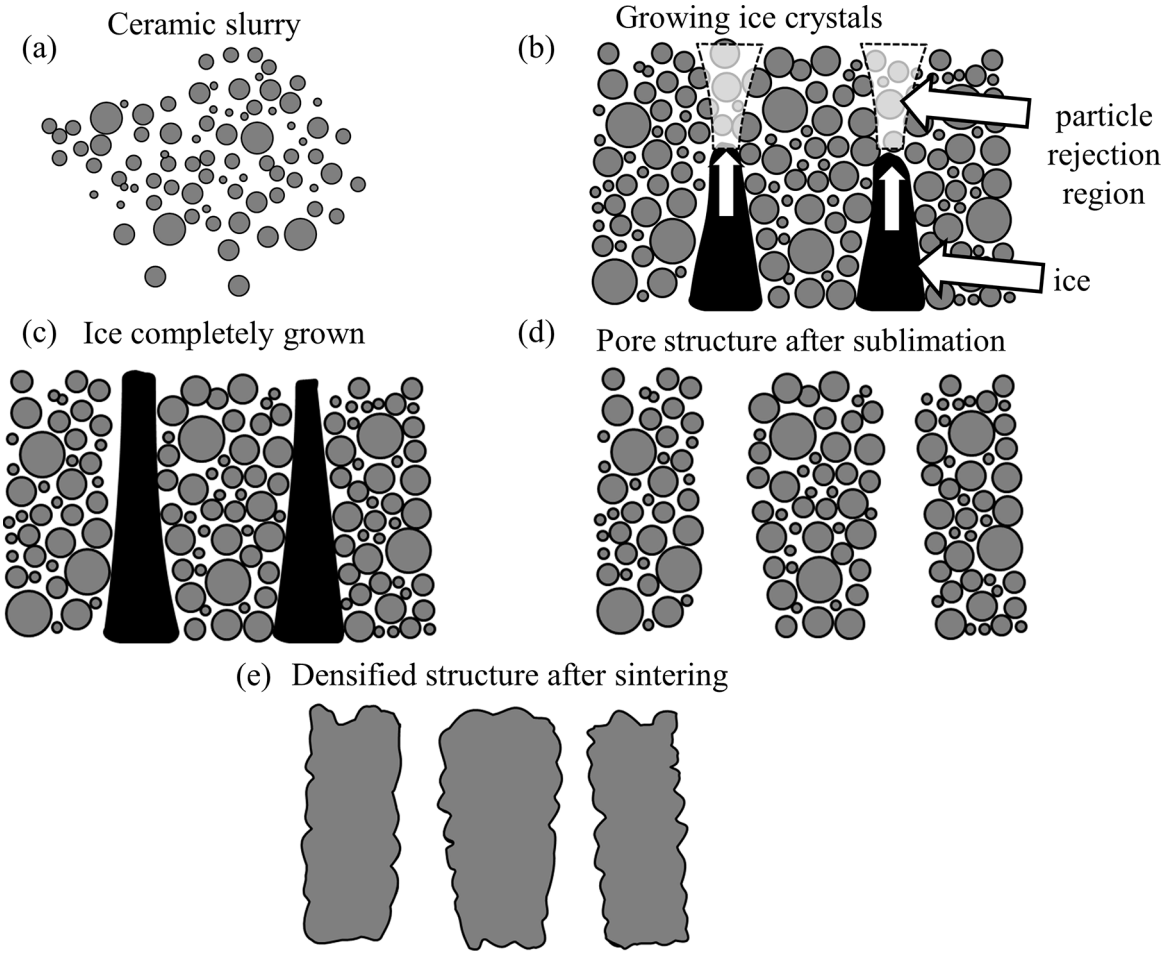

Figure 1. Schematic illustration of the freeze-casting process followed by the heat treatment for production of ceramic substrates (Adapted from [13]).

of the formed ice crystal and, consequently on the pore structure [13,14]. The frozen sample is then submitted to low pressures (i.e. ~50 µm-Hg for aqueous ceramic suspension) to induce solvent sublimation, converting the solidified solvent directly to the gas phase. The region occupied by the solvent crystals will form the organized macropore structure. Finally, the sample is heat treated to guarantee a consolidated and robust ceramic material [13,15,16]. The result is a final structure with an organized and aligned porosity. Typically, the pore structure exhibit high open porosity with low tortuosity, indicating great potential for fluid permeation applications. In fact, several papers have assessed the fluid permeation on freeze-cast substrates with impressive results [1,17,18].

When considering production of freeze-cast substrates for membrane production, the tubular geometry is more appropriate than flat supports. The tubular geometry shows higher surface area to volume ratio, allowing higher flow rates for similar membrane modules[11]. It also allows a radially aligned pore structure, which is more indicated for fluid permeation and has been confirmed to improve the mechanical strength of ceramic substrates [19]. Nevertheless, only a few studies have reported the production of freeze-cast tubular supports [17,20,21], and, to the best of authors' knowledge, none of them report the use of water as solvent. Furthermore, the lack of discussion about the production of a top porous film on the tubular freeze-cast substrates indicates the necessity for further studies. The deposition of a homogeneous separation layer on the macroporous substrates might be challenging due to the great differences in pore sizes between the substrate (>50 nm) and the top layer (<2 nm), sometimes demanding several depositions (1-5 layers) for production of a homogeneous and flawless top layer [11].

The sol-gel route can be used for production of the separation layer, since it has been proven as an efficient method for production of high-quality silica membranes [22,23]. It allows precise control of the pore structure (shape and pore size distribution) [24,25,26], a desired characteristic for membrane production. In addition, it is a suitable route for thin film deposition, due to the capability to coat materials of various shapes and areas, as well as demanding low temperatures and simple equipment [22,24,27]. For production of microporous

silica layer, acidic synthesis conditions and short aging times are preferred before deposition [25]. The use of dip-coating for production of sol-gel derived silica coatings has shown its capability to produce homogeneous layer [24,28]. According to the Landau-Levich equation [28], the dip coating method allows control of the film thickness by adjusting the withdrawal speed [29].

In this study, a novel freeze-cast tubular substrate was used for production of an asymmetric membrane with potential for nanofiltration applications. The alumina substrates were produced using water as solvent in order to obtain a sustainable material. Silica sol-gel [30] was chosen as separation layer and deposited by the dip-coating technique. Two different withdrawal speeds were used for deposition of the silica layer. Characterization of the pore structure was performed by microscopy and nitrogen adsorption. The results allowed estimation of the most adequate parameters for production of a homogeneous separation layer on the freeze-cast substrates.

2. Experimental

Freeze-cast tubular substrates were manufactured using a commercial alumina (Almatis - Alumina CT 3000 SG). A water-based ceramic suspension was prepared using 20 vol% solid concentration. Sodium polyacrylate (Sigma-Aldrich) was used as dispersant agent and polyvinyl alcohol (Sigma-Aldrich) was used as a binder. All reagents were mixed in water and kept stirring for 24 hours. The suspension was poured in a tubular copper mold and immerged in liquid nitrogen (T ≈ -197°C) to freeze the solvent. The mold was prepared in a way to guarantee one single cold front from the outer side of the tube. The frozen alumina substrates were freeze-dried (Liotop L101 series) at low pressures (within 50-80 μmHg) for 24 hours until complete solvent (water) sublimation. The green bodies were heat treated at 1500 °C in a conventional furnace (Thermolab) for 1 hour. Heating and cooling rates in the furnace were kept at 2 °C/min. After sintering, the freeze-cast tubes showed average values of external and internal diameter of 10.74 mm and 6.70 mm, respectively, as well as width varying within 40-45 mm.

The silica layer was produced based on a sol-gel route previously reported [1,30]. As shown in Figure 2, deionized water, ethanol (Sigma-Aldrich), nitric acid (65 %, Synth) and tetraethyl orthosilicate (TEOS, 98 %, Sigma-Aldrich) were mixed together and left stirring at 90 °C for 3 hours under reflux. The silica sol was then divided in two parts. The first was used to produce an unsupported membrane by pouring a thin film of the sol into a petri dish for further characterization of the structure and the thermal behavior. The second part of the silica sol was used in the production of a supported membrane by impregnating the alumina tube with the silica sol by dip-coating. The film deposition was

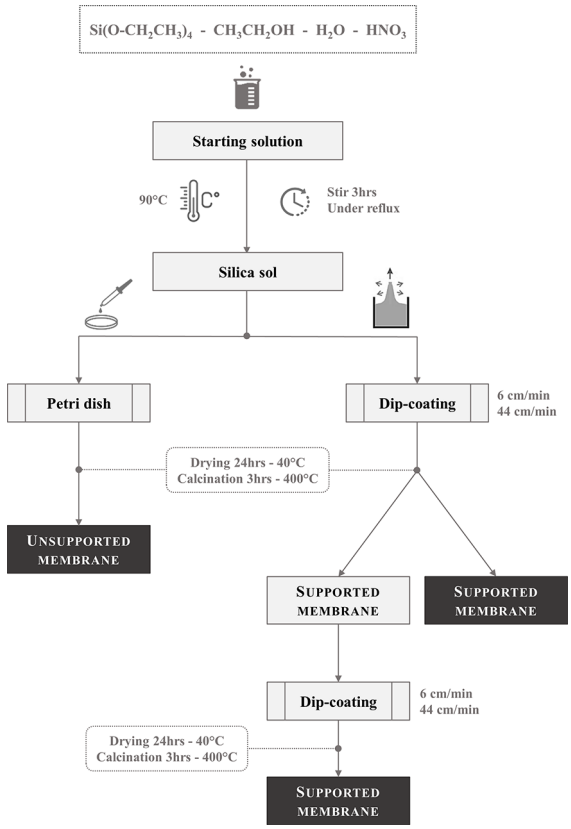

Figure 2. Schematic diagram of the silica membrane preparation.

performed on the outer surface of the tube. A dip-coater (CONSTRUMAQ) was used and the tubular substrates were kept immersed for 30 seconds. The immersion and drainage stages were performed using two different withdrawal speeds: 6 and 44 cm/min. Both membranes were dried at 40 °C for 24 hours. Finally, they were heat treated in a conventional furnace (Thermolab) for 3 hours in air at 400 °C with heating and cooling rates of 1 °C/min. The dip-coating stage was repeated once to assess the influence of the number of depositions on the characteristics of the silica top layer. Despite the obvious differences between the gelation and drying conditions of the supported and the unsupported silica film, it has already been found a strong correlation between the properties of films and bulk gels [1,31,32]. In other words, the unsupported silica film can be used as an estimation of the pore structure of the produced silica film on the freeze-cast substrate. This comparison will also be done in this study.

The pore structure of the freeze-cast substrates was characterized by scanning electron microscopy (SEM, Quanta FEG 3D FEI). The SEM images were treated on the ImageJ software using the OrientationJ plugin to measure the directionality and the pore directionality distribution. This plugin has already been reported on the literature [33,34]. The Archimedes' method, as described in ASTM B962-13 [35], was used to assess the open porosity. Also, mercury intrusion

porosimetry (Micromeritics - Autopore IV) using pressures ranging within 0.02-4123 bar allowed estimation of the pore size distribution.

Thermogravimetric analysis (TGA) of the unsupported silica film was carried out in a Perkin-Elmer STA-6000 thermal analyzer. The silica powder was heated to 900 °C using a heating rate of 5 °C/min in synthetic air. The heat treated (at 400 °C) unsupported silica was also compared with the dried gel and the sol-gel solution by Fourier transform infrared spectroscopy (FTIR, Perkin-Elmer - Frontier) with ATR accessory in the range of 4000-400 cm^{-1}. The pore structure of the unsupported silica was assessed by a nitrogen adsorption equipment (Quantachrome Autosorb 1C). Finally, the top view of the silica layer was characterized by scanning electron microscope (ASPEX - Explorer) using backscattered electrons in order to assess the alumina substrate coverage.

3. Results and Discussion

The freeze-cast substrates showed an organized structure with radially aligned porosity, as shown in Figure 3 (a and b). As one may notice, most pores connect the inner and the outer sides of the wall, indicating high open porosity. Assessment of the open porosity by the Archimedes' method confirms that the open porosity is around 67.6 %, a high value that is favorable to fluid permeation. The pore walls were considered robust, with absence of wholes and cracks on it. It was also possible to notice the formation of ceramic bridges between the pore walls (Figure 3c), similar to the structure reported by Deville [13]. This is a clear indication of the complex structure formed during freeze-casting, which improves the mechanical stability of freeze-cast substrates

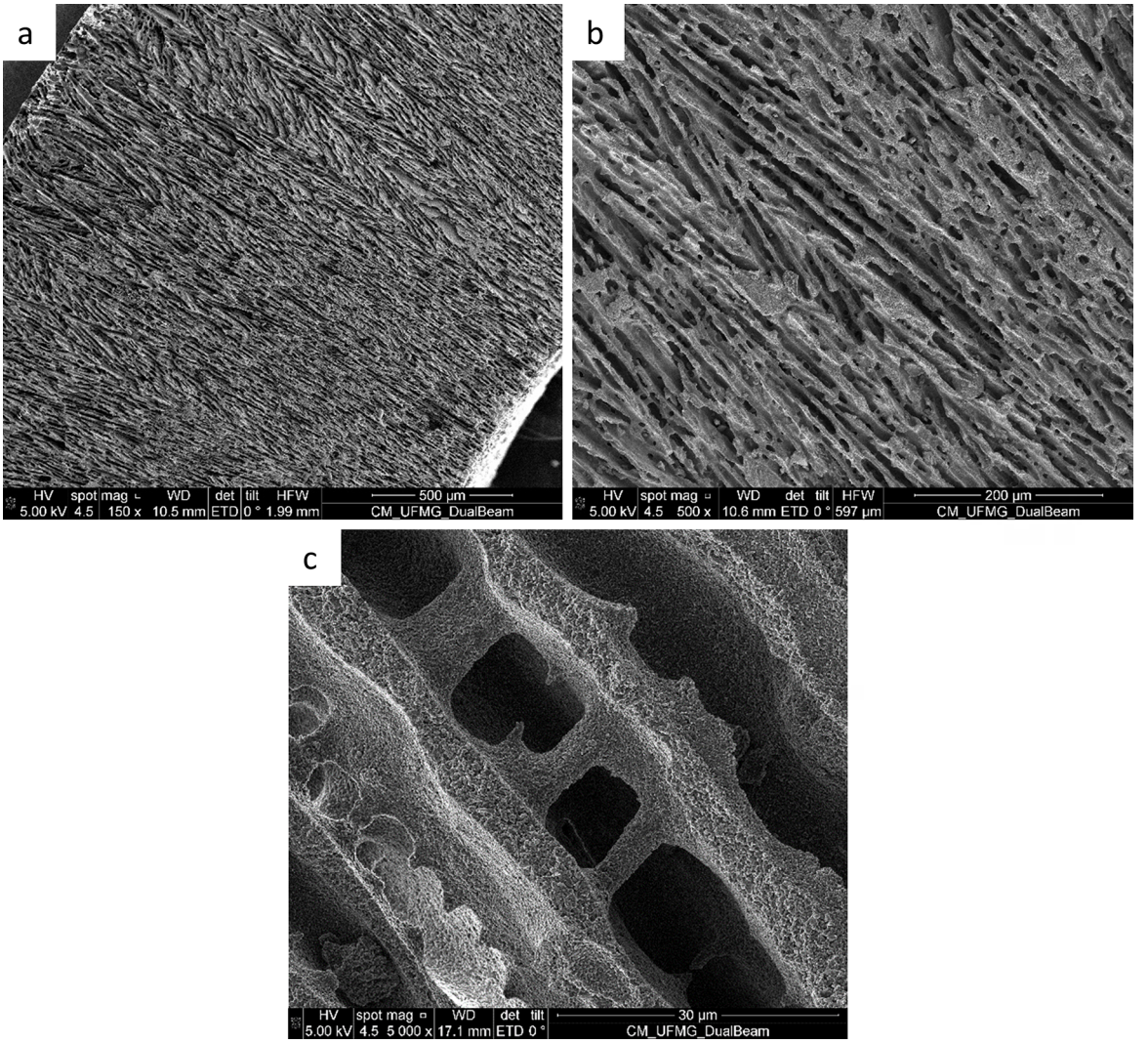

Figure 3. Tubular alumina substrates: (a) and (b) showing radially aligned porosity at different magnifications, and (c) the trans-lamellar ceramic bridges.

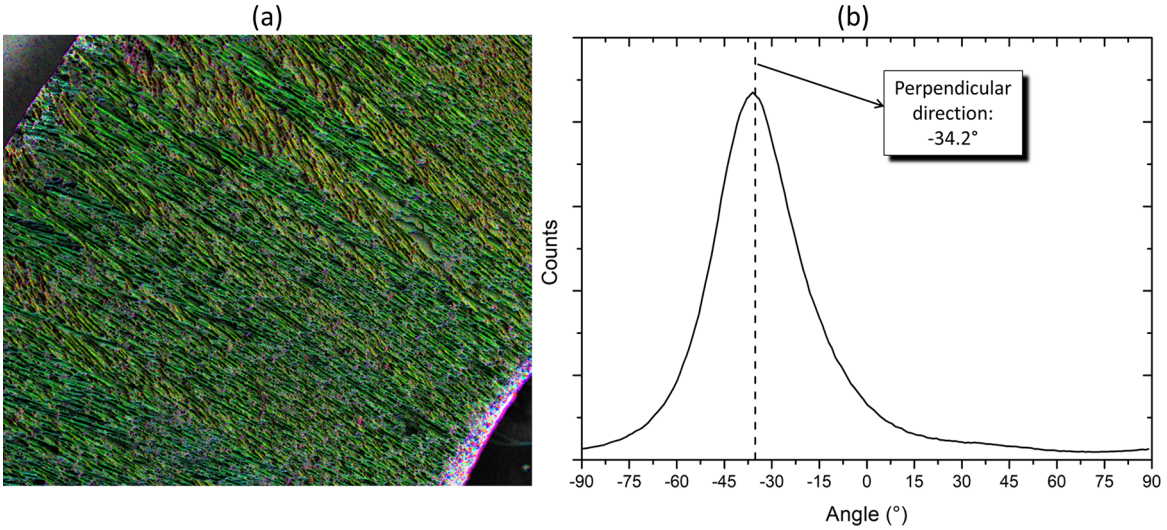

Figure 4. Pore directionality of the freeze-cast pores measured by the OrientationJ plugin on ImageJ: (a) color map of the pore directionality and (b) pore directionality distribution.

and produces a material suitable to withstand pressures commonly used in membrane applications (Table 1).

An analysis of the pore directionality by the OrientationJ plugin on ImageJ [33,34] allowed assessment of the angles of the pores shown in Figure 3(a). The results of the pore directionality and the pore directionality distribution are shown in Figure 4. In Fig. 4(a), it is possible to notice that most pores are in the same direction and, thus, highlighted as green in the image. A few regions, highlighted with yellow color, show pores with slightly different angles. Assessment of the pore directionality, as shown in Fig. 4(b) confirmed that most pores are concentrated in the perpendicular direction when compared to the tube's surface. It is worth mentioning that the perpendicular direction was measured based on the mean angle of the two surfaces of the tube wall. As one may notice in Figure 5, the pore size distribution shows a sharp peak, with pore sizes varying within 4-20 µm and average size of 7.05 µm. Moreover, the total pore volume is 0.48 cm^3/g, a result considerably high when compared with substrates produced by conventional methods [36]. These results confirm the high level of structure control of substrates produced by the freeze-casting and indicate that the substrate will show low resistance for mass transport.

The thermal behavior of the silica unsupported film was assessed by thermogravimetric analysis and the result is shown in Figure 6. The sharp mass loss observed in the DTG curve at around 100 °C is attributed to evaporation of residual free-water and ethanol in the film structure. These are derived from additions in the sol-gel synthesis and from condensation reactions during the silica network formation. This first mass loss step corresponds to a loss of 18 % in the TG curve. The mass loss continues until 180 °C and can be associated to the evaporation of water inside the pore structure and desorption of physically-adsorbed water. The mass losses at higher temperatures (~300 °C) can be attributed to thermal decomposition of remaining organic compounds such as the ethyl radical of unreacted TEOS. The elimination of hydrogen-bonded hydroxyls (-OH) from the silica surface (dihydroxylation process) resulted in a fast

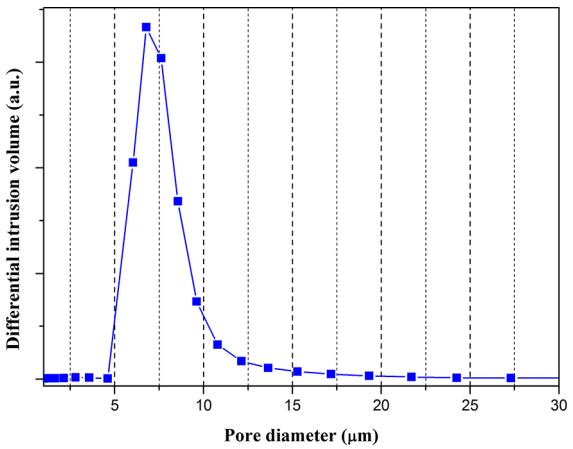

Figure 5. Pore size distribution of the alumina substrate by mercury intrusion porosimetry.

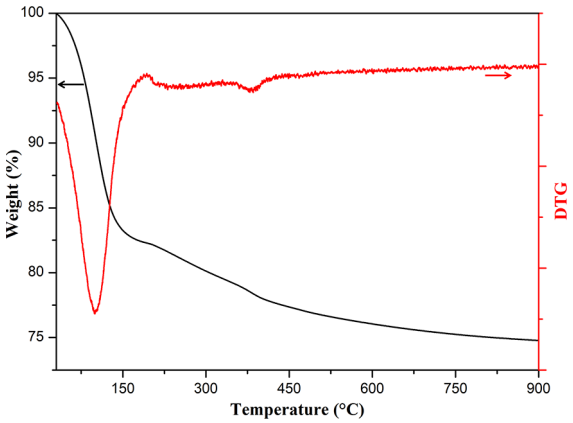

Figure 6. TG-DTG curves of unsupported silica film dried at 40 °C.

mass loss at 400 °C, as one may notice in the DTG curve. Above 400 °C, the unsupported silica film kept losing mass at a lower rate, which is attributed to the dihydroxylation of isolated hydroxyls groups in the silica structure [37]. In this last region, amorphous silica typically shrinks intensively, increasing the possibility of crack formation on the film [38]. The TG curve shows that the sample showed a total mass loss of 25.2 %. Due to thermal behavior of the unsupported silica film, and based on previous studies [1,30], the calcination temperature was kept at 400 °C. This temperature guarantees degradation of organic compounds and does not cause high shrinkage of the silica film. Also, the calcination temperature has a great impact on the pore size distribution [39], since higher calcination temperatures lead to elimination of smaller pores and, consequently, an increase on average pore size. The goal of this study is to produce a microporous separation layer, hence, the chosen temperature must be low enough to guarantee the presence of micropores on the silica top layer.

The elimination of organic compounds when the sample was heat treated at 400 °C for 3 hours is confirmed by the FTIR spectra, as shown in Figure 7. The silica sol spectrum displays a variety of bands typical of the reagents used on the sol-gel process [40], as detailed in Table 2. The band at 430 cm^{-1} confirms that the silica structure has already been formed by the condensation reactions. After drying at 40 °C for 24 hours the spectra changed significantly, showing bands attributed to silanol (Si-O-H) and siloxane (Si-O-Si) groups, as detailed in Figure 7. The band attributed to the silanol group is easily distinguished from other bands, indicating that structural water is still present on the silica structure. After the heat treatment at 400 °C, the Si-O-Si bands intensities were significantly increased indicating that the heat treatment was effective on the structure development of silica network. Also, the heat treatment allowed complete elimination of residual organic compounds. This is important for porous materials, since the presence of organic molecules might occupy and block the pores, hence decreasing the surface area [38,41]. This phenomenon hinders the fluid transport through membranes. Thus, the absence of organic compounds indicates that the pores on the silica film are free and will be available to fluid transport.

Analysis of the unsupported film by nitrogen adsorption, Figure 8, showed that the silica layer exhibited a Type I isotherm according to the IUPAC classification [42,43]. This is typical of microporous materials with exposed surface area composed almost exclusively inside the micropores. Once

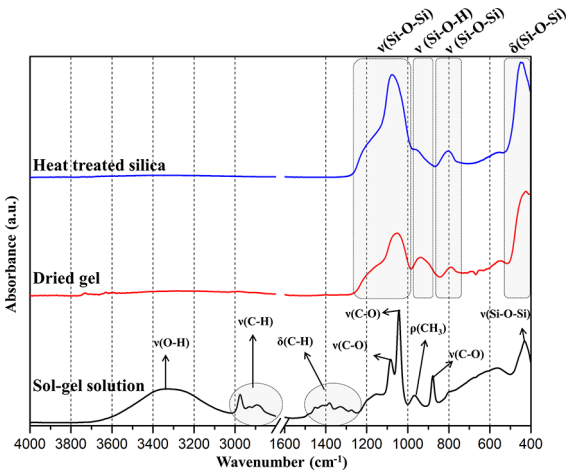

Figure 7. FTIR spectra of the silica sol, the gel dried at 40 °C for 24 hours and the silica layer heat treated at 400 °C for 3 hours. The symbols are attributed to stretching (ν), bending (δ) and rocking vibration (ρ).

Table 2. Assignments of absorption frequencies of FTIR spectra of silica sol [40]. The symbols are attributed to stretching (ν), bending (δ) and rocking vibration (ρ).

Wavenumber (cm^{-1})	Vibrational assignments
3600-3100	ν(O-H) bonds on free water
3000-2800	ν(C-H) in the $CH_2$and CH_3groups
1500-1250	δ(C-H)
1080	ν(C-O) from the TEOS structure
1043	ν(C-O) from the ethanol
965	ρ(CH_3) from TEOS
878	ν(C-O) from ethanol
430	δ(Si-O-Si)

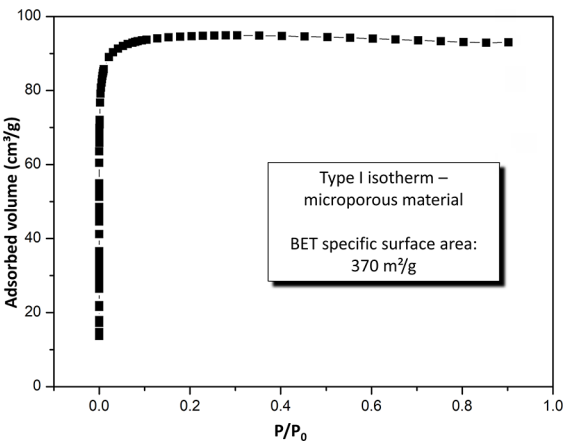

Figure 8. Nitrogen adsorption isotherm of the silica layer.

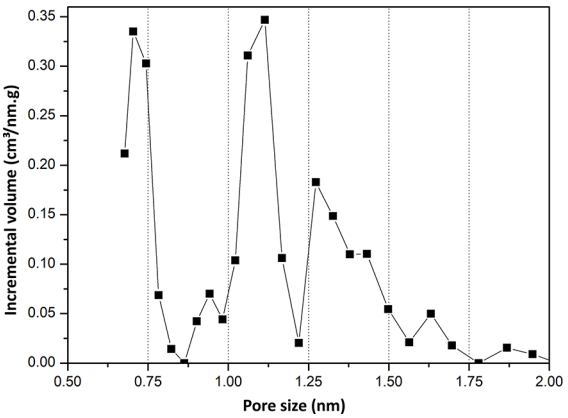

Figure 9. Pore size distribution of the silica layer by DFT method.

these are filled with adsorbate, there is little or no external surface remaining for further adsorption [44]. This was confirmed by the BET analysis, which resulted in a specific surface area of 370 m^2/g. The NLDFT method allowed estimation of pore size distribution, confirming the presence of micropores (< 2 nm) on the silica layer. Three main peaks were visible in the pore size distribution (Figure 9) showing maximum values at 0.70, 1.11 and 1.27 nm. All pores were smaller than 2 nm, suggesting that membranes produced using this silica layer as separation layer may be applied for nanofiltration membranes (Table 1). For instance, this pore size has been proven to be used for efficient separation of He/CO_2 and He/N_2 systems [1]. Since the sol-gel process is known to show accurate control of the pore structure [25,26], deposition of a sol-gel silica membrane on the tubular freeze-cast substrate can lead to an unlimited number of applications.

Figure 10 displays the SEM images of the final supported membranes with the different withdrawal speeds for one and two dip-coating depositions. The membranes produced with the withdrawal speed of 6 cm/min showed lower substrate coverage. In the first deposition, Fig 10(a), the silica film was visible only in some regions and the pore structure of the substrate was almost completely exposed. Even with a second dip-coating deposition, Fig 10(b), the substrate was not completely covered, and some pores were still exposed. As for the sample with the withdrawal speed of 44 cm/min shown in Fig. 10(c), the substrate was more widely covered. Only a few macropores typical of the freeze-cast substrate were visible. After the second deposition, Fig. 10(d), the silica film completely covered the freeze-cast substrate, forming a homogeneous film and guaranteeing a uniform separation layer. The influence of the withdrawal speed on

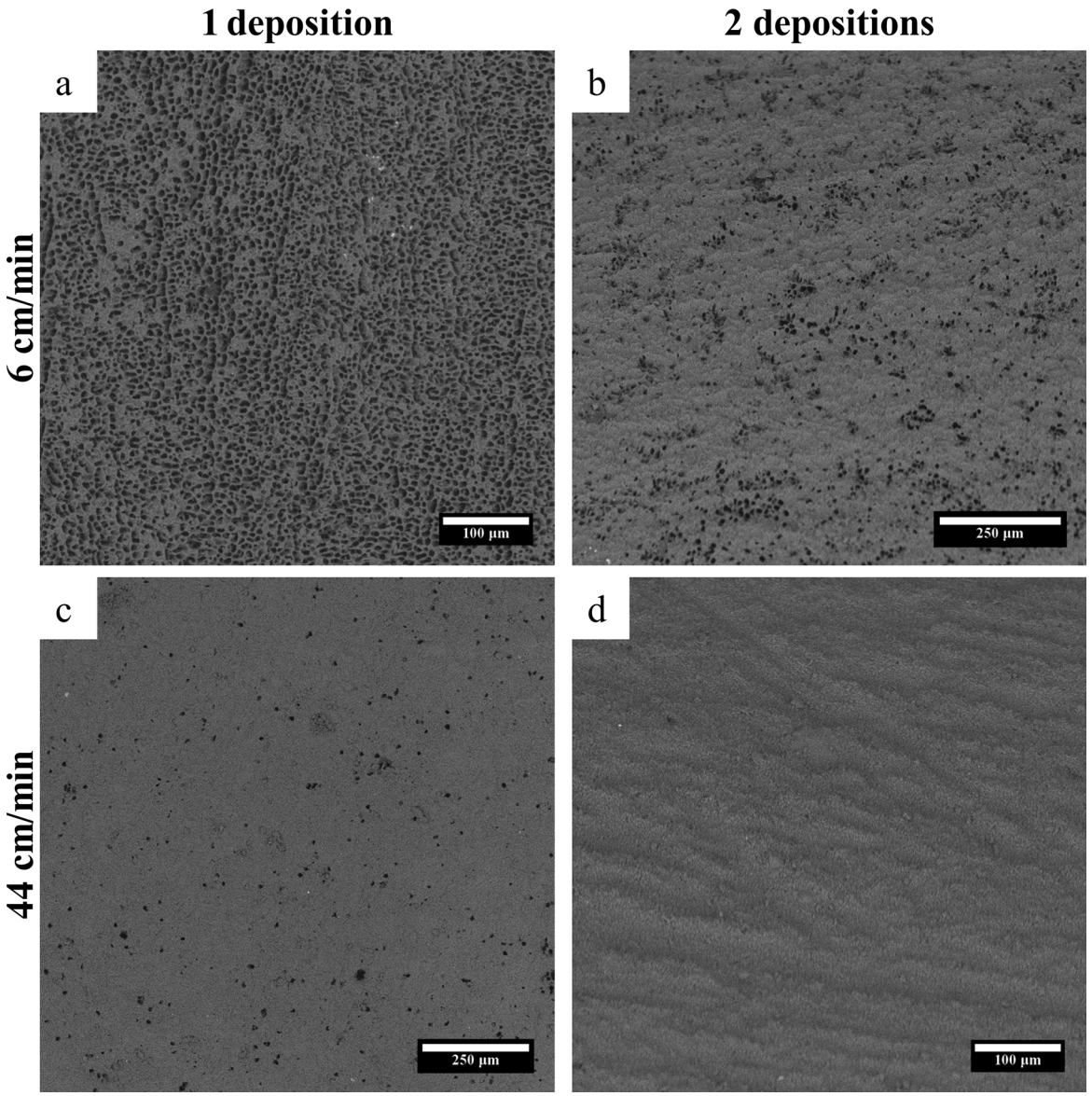

Figure 10. SEM images (backscattered electrons) detailing the deposition of the silica top layer on the freeze-cast substrates.

the substrate coverage is in accordance with the Landau-Levich equation [28], which stablishes that for withdrawal speeds higher than 6 cm/min the film thickness increases with the withdrawal speed increase. This correlation is often reported for sol-gel film deposition and is attributed to the many parameters involved, such as evaporation rate, viscous drag, gravity forces and liquid-vapor surface tension [28,29].

As one may notice in Figure 10(d), after two depositions of the silica sol using the fastest speed the membrane is homogeneous and without visible cracks. Thus, it indicates that the membrane has potential to be used for separation purposes. This is an outstanding result, since deposition of a film with pore sizes extremely different from the sizes found on the substrate tends to form cracks [11]. Moreover, the drying stage of the dip-coated film happens faster, leading to gelation of the sol by solvent evaporation instead of the condensation reactions involved on the sol-gel process. The result is a gel more weakly condensed that could increase the formation of cracks [28]. Regarding the film thickness, it was not possible to determine an accurate value. The silica sol penetrated on the freeze-cast pore structure forming a silica layer inside the alumina macropores. Thus, there was an overlap of the alumina substrate and the silica, making it difficult to distinguish the two materials and assess the film thickness. The authors suggest that the penetration of the silica membrane into the alumina macropores contributed to a better film-substrate adhesion, guaranteeing sufficient resistance to the silica membrane to be used without detachment from the tubular freeze-cast substrates.

4. Conclusions

The study confirmed that the production of tubular alumina substrates by the freeze-casting technique allows precise control of the pore structure. An aligned and organized porosity was obtained with most of the pores on the perpendicular direction. The radially aligned pore structure showed high pore volume when compared to substrates produced by conventional methods. In addition, the freeze-casting method allowed production of substrates with sharp pore size distribution. Thus, the freeze-cast substrates showed high potential for fluid permeation applications, such as for membrane fabrication. As for the silica layer produced by sol-gel, TGA and FTIR analysis showed that the heat treatment guarantees elimination of the organic compounds, while minimizing shrinkage and densification of the top layer. The sol-gel route allowed synthesis of a silica membrane with microporous (pore diameter < 2 nm) structure. SEM images of the silica top layer revealed that the withdrawal speed has a great influence on the membrane formation. As predicted by the Landau-Levich equation, the highest withdrawal speed produced a silica layer with greater substrate coverage. However, a second deposition was necessary in order to guarantee an uniform silica membrane. Despite the difficulties involved on the production of a uniform microporous film on a macroporous substrate (due to the large difference between the pore sizes), the silica layer did not present any cracks. Thus, the membrane produced in this study confirms that the tubular freeze-cast substrates can be used for production of asymmetric membranes. The use of the novel tubular geometry indicates the capacity of the freeze-casting for widespread use on industrial processes. Finally, this study confirms high potential of the freeze-cast substrates for deposition of microporous films and, consequently, for manufacture of nanofiltration membranes.

5. Acknowledgement

The authors gratefully thank the financial support from Brazilian agencies Capes-Proex (433/2010) and CNPq (401793/2013-3).The authors would like to acknowledge the Center of Microscopy at the Universidade Federal de Minas Gerais (http://www.microscopia.ufmg.br) for providing the equipment and technical support for experiments involving electron microscopy. The authors also thank Vale S.A. for performing the Hg-porosimetry tests. D. D. Athayde acknowledges the financial support by the Pró-reitoria de Pesquisa from Universidade Federal de Minas Gerais for the article processing charge.

6. References

1. Souza DF, Nunes EHM, Pimenta DS, Vasconcelos DCL, Nascimento JF, Grava W, et al. Synthesis and structural evaluation of freeze-cast porous alumina. *Materials Characterization*. 2014;96:183-195.

2. Wei W, Qin G, Hu H, You L, Chen G. Preparation of supported carbon molecular sieve membrane from novolac phenol-formaldehyde resin. *Journal of Membrane Science*. 2007;303(1-2):80-85.

3. Zainal WNHW, Tan SH, Ahmad MA. Carbon Membranes Prepared from a Polymer Blend of Polyethylene Glycol and Polyetherimide. *Chemical Engineering Technology*. 2017;40(1):94-102.

4. Wijaya S, Duke MC, Diniz da Costa JC. Carbonised template silica membranes for desalination. *Desalination*. 2009;236(1-3):291-298.

5. Koros WJ, Ma YH, Shimidzu T. Terminology for membranes and membrane processes (IUPAC Recommendations 1996). *Pure and Applied Chemistry*. 1996;68(7):1479-1489.

6. Cheryan M. *Ultrafiltration and Microfiltration Handbook*. Boca Raton: CRC Press; 1998.

7. Valentas KJ, Rotstein E, Singh RP, eds. *Handbook of Food Engineering Practice*. Boca Raton: CRC Press; 1997.

8. Shon HK, Phuntsho S, Chaudhary DS, Vigneswaran S, Cho J. Nanofiltration for water and wastewater treatment - a mini review. *Drinking Water Engineering and Science*. 2013;6:47-53.

9. Jalil SNA, Wang DK, Yacou C, Motuzas J, Smart S, Diniz da Costa JC. Vacuum-assisted tailoring of pore structures of phenolic resin derived carbon membranes. *Journal of Membrane Science*. 2017;525:240-248.

10. Queiroga JA, Souza DF, Nunes EHM, Silva AFR, Amaral MCS, Ciminelli VST, et al. Preparation of alumina tubular membranes for treating sugarcane vinasse obtained in ethanol production. *Separation and Purification Technology*. 2018;190:195-201.

11. Burggraaf AJ, Cot L, eds. *Fundamentals of Inorganic Membrane Science and Technology*. Amsterdam: Elsevier Science; 1996.

12. Scotti KL, Dunand DC. Freeze casting - A review of processing, microstructure and properties via the open data repository, FreezeCasting.net. *Progress in Materials Science*. 2018;94:243-305.

13. Deville S. Freeze-Casting of Porous Ceramics: A Review of Current Achievements and Issues. *Advanced Engineering Materials*. 2008;10(3):155-169.

14. Delattre B, Amin R, Sander J, De Coninck J, Tomsia AP, Chiang YM. Impact of Pore Tortuosity on Electrode Kinetics in Lithium Battery Electrodes: Study in Directionally Freeze-Cast $LiNi_{0.8}Co_{0.15}Al_{0.05}O_2$ (NCA). *Journal of the Electrochemical Society*. 2018;165(2):A388-A395.

15. Gaudillere C, Serra JM. Freeze-casting: Fabrication of highly porous and hierarchical ceramic supports for energy applications. *Boletín de la Sociedad Española de Cerámica y Vidrio*. 2016;55(2):45-54.

16. Liu R, Xu T, Wang CA. A review of fabrication strategies and applications of porous ceramics prepared by freeze-casting method. *Ceramics International*. 2016;42(2 Pt B):2907-2925.

17. Liu R, Yuan J, Wang CA. A novel way to fabricate tubular porous mullite membrane supports by TBA-based freezing casting method. *Journal of the European Ceramic Society*. 2013;33(15-16):3249-3256.

18. Gaudillere C, Garcia-Fayos J, Serra J. Enhancing oxygen permeation through hierarchically-structured perovskite membranes elaborated by freeze-casting. *Journal of Materials Chemistry A*. 2014;2(11):3828-3833.

19. Tang Y, Miao Q, Qiu S, Zhao K, Hu L. Novel freeze-casting fabrication of aligned lamellar porous alumina with a centrosymmetric structure. *Journal of the European Ceramic Society*. 2014;34(15):4077-4082.

20. Moon JW, Hwang HJ, Awano M, Maeda K. Preparation of NiO-YSZ tubular support with radially aligned pore channels. *Materials Letters*. 2003;57(8):1428-1434.

21. Dong S, Zhu W, Gao X, Wang Z, Wang L, Wang X, et al. Preparation of tubular hierarchically porous silicate cement compacts via a tert-butyl alcohol (TBA)-based freeze casting method. *Chemical Engineering Journal*. 2016;295:530-541.

22. Danks AE, Hall SR, Schnepp Z. The evolution of 'sol-gel' chemistry as a technique for materials synthesis. *Materials Horizons*. 2016;3:91-112.

23. Yang H, Wang DK, Motuzas J, Diniz da Costa JC. Hybrid vinyl silane and P123 template sol-gel derived carbon silica membrane for desalination. *Journal of Sol-Gel Science and Technology*. 2018;85(2):280-289.

24. Silva DG, Costa VC, Nunes RAX. Preparation of Antireflective Silica Coating by the Sol-Gel Method for Heliothermic Power Plants. *Materials Research*. 2018;21(3):e20170970.

25. Levy D, Zayat M, eds. *The Sol-Gel Handbook: Synthesis, Characterization and Applications*. Hoboken: John Wiley & Sons; 2015.

26. Sakka S, ed. *Handbook of Sol-Gel Science and Technology: Processing, Characterization and Applications*. Boston: Kluwer Academic Publishers; 2005.

27. Niederberger M, Pinna N. *Metal Oxide Nanoparticles in Organic Solvents: Synthesis, Formation, Assembly and Application*. London: Springer-Velag; 2009.

28. Brinker CJ. Dip Coating. In: Schneller T, Waser R, Kosec M, Payne D, eds. *Chemical Solution Deposition of Functional Oxide Thin Films*. Wien: Springer-Verlag Wien; 2013. p. 234-261.

29. Han Y, Na YH. Measurement of liquid film thickness on moving plate during dip-coating process. *Korea-Australia Rheology Journal*. 2018;30(2):137-143.

30. Uhlhorn RJR, Keizer K, Burggraaf AJ. Gas transport and separation with ceramic membranes. Part II. Synthesis and separation properties of microporous membranes. *Journal of Membrane Science*. 1992;66(2-3):271-287.

31. Song Y, Wang DK, Birkett G, Martens W, Duke MC, Smart S, et al. Mixed Matrix Carbon Molecular Sieve and Alumina (CMS-Al_2O_3) Membranes. *Scientific Reports*. 2016;6:30703.

32. Brinker CJ, Mukherjee SP. Comparisons of sol-gel derived thin films with monoliths in a multicomponent silicate glass system. *Thin Solid Films*. 1981;77(1-3):141-148.

33. Püspöki Z, Storath M, Sage D, Unser M. Transforms and Operators for Directional Bioimage Analysis: A survey. *Advances in Anatomy, Embryology, and Cell Biology*. 2016;219:69-93.

34. Rezakhaniha R, Agianniotis A, Schrauwen JTC, Griffa A, Sage D, Bouten CVC, et al. Experimental investigation of collagen waviness and orientation in the arterial adventitia using confocal laser scanning microscopy. *Biomechanics and Modeling in Mechanobiology*. 2012;11(3-4):461-473.

35. ASTM International. *ASTM B962-13 - Standard Test Methods for Density and Compacted or Sintered Powder Metallurgy (PM) Products Using Archimedes' Principle*. West Conshohocken: ASTM International; 2013.

36. Queiroga JA, Nunes EHM, Souza DF, Vasconcelos DCL, Ciminelli VST, Vasconcelos WL. Microstructural investigation and performance evaluation of slip-cast alumina supports. *Ceramics International*. 2017;43(4):3824-3830.

37. EK S, Root A, Peussa M, Niinistö L. Determination of the hydroxyl group content in silica by thermogravimetry and a comparison with $_1$H MAS NMR results. *Thermochimica Acta*. 2001;379(1-2):201-212.

38. Brinker CJ, Scherer GW. Structural changes during heating: amorphous systems. In: Brinker CJ, Scherer GW. *Sol-Gel Science - The Physics and Chemistry of Sol-Gel Processing*. Boston: Academic Press; 1990.

39. Xi Y, Liangying Z, Sasa W. *Pore size and pore-size distribution control of porous silica*. Sensors and Actuators B: Chemical. 1995;25(1-3):347-352.

40. Tejedor-Tejedor MI, Paredes L, Anderson MA. Evaluation of ATR-FTIR Spectroscopy as an "in Situ" Tool for Following the Hydrolysis and Condensation of Alkoxysilanes under Rich H_2O Conditions. *Chemistry of Materials*. 1998;10(11):3410-3421.

41. Kwon S, Pignatello JJ. Effect of Natural Organic Substances on the Surface and Adsorptive Properties of Environmental Black Carbon (Char): Pseudo Pore Blockage by Model Lipid Components and Its Implications for N_2-Probed Surface Properties of Natural Sorbents. *Environmental Science & Technology*. 2005;395(20):7932-3939.

42. Sing KSW, Everett DH, Haul RAW, Moscou L, Pierotti RA, Rouquérol J, et al. Reporting Physisorption Data for Gas/Solid Systems With Special Reference to the Determination of Surface Area and Porosity (Recommendations 1984). *Pure and Applied Chemistry*. 1985;57(4):603-619.

43. Thommes M, Kaneko K, Neimark AV, Olivier JP, Rodriguez-Reinoso F, Rouquerol J, et al. Physisorption of gases with special reference to the evaluation of surface area and pore size distribution (IUPAC Technical Report). *Pure and Applied Chemistry*. 2015;87(9-10):1051-1069.

44. Anovitz LM, Cole DR. Characterization and Analysis of Porosity and Pore Structures. *Reviews in Mineralogy and Geochemistry*. 2015;80(1):61-164.